

Article

# Effect of Pristine Palygorskite Powders on Explosion Characteristics of Methane-Air Premixed Gas

Yimin Zhang<sup>1,2</sup>, Yan Wang<sup>1,2,\*</sup> , Ligang Zheng<sup>1,2</sup>, Tao Yang<sup>3</sup>, Jianliang Gao<sup>1,2</sup> and Zhenhua Li<sup>1,\*</sup>

<sup>1</sup> The Collaboration Innovation Center of Coal Safety Production of Henan Province, Henan Polytechnic University, Jiaozuo 454000, China; zhangyimin2018@gmail.com (Y.Z.); li.g.zhang@hpu.edu.cn (L.Z.); gao@hpu.edu.cn (J.G.)

<sup>2</sup> State Key Laboratory Cultivation Bases for Gas Geology and Gas Control, College of Safety Science and Engineering, Henan Polytechnic University, Jiaozuo 454000, China

<sup>3</sup> School of Safety Engineering, North China Institute of Science & Technology, Sanhe 065201, China; yangtao@ncist.edu.cn

\* Correspondence: yanwang@hpu.edu.cn (Y.W.); lizh@hpu.edu.cn (Z.L.); Tel.: +86-391-398-7440 (Y.W. & Z.L.)

Received: 24 August 2018; Accepted: 17 September 2018; Published: 20 September 2018



**Abstract:** In this study, pristine palygorskite powders were used as the inhibition materials to suppress the explosion of methane-air premixed gas for the first time. The composition, porosity and pyrolysis characteristics of the powders were tested by X-ray diffraction (XRD), energy dispersive spectrometry (EDS), N<sub>2</sub> adsorption-desorption and Thermogravimetry-differential scanning calorimetry (TG-DSC) techniques. The effects of pristine palygorskite powders concentration on the explosion pressure and the average velocity of flame propagation of the 9.5% methane-air premixed gas were tested by a 20 L spherical explosion system and a 5 L pipeline explosion system. The results indicated the pristine palygorskite powders possess a considerable suppression property on methane explosion. When the mass concentration of pristine palygorskite powders was 0.20 g·L<sup>-1</sup>, the max-pressure of methane explosion was decreased by 23.9%. The methane explosion flame propagation velocity was inhibited obviously. Owing to the excellent inhibitory performance and the advantage of low-cost and environmental harmlessness, pristine palygorskite powders are potential new materials for the application on gas explosion suppression.

**Keywords:** pristine palygorskite powders; methane explosion; explosion suppression; explosion parameters

## 1. Introduction

As is known, there are abundant coal resources in China. However, the complex deposit condition and the harsh production environment lead to the frequent occurrence of coal mine disasters. The gas explosion is one kind of major disasters, which seriously affects the safety of coal mine workers and the economic development of the coal industry. In recent years, researchers have made some progress in the technologies and materials for suppressing gas explosion. Chemical powders, aerosol, water mist and inert gases [1–6] were used for preventing the gas explosion. Due to the outstanding suppression effect, chemical powders have become a new research focus in the field of gas explosion suppression. Among them, SiO<sub>2</sub>, NH<sub>4</sub>H<sub>2</sub>PO<sub>4</sub>, CaCO<sub>3</sub>, NaHCO<sub>3</sub>, KHCO<sub>3</sub>, Al(OH)<sub>3</sub>, Fe(OH)<sub>3</sub>, Mg(OH)<sub>2</sub>, NaCl, CO(NH<sub>2</sub>)<sub>2</sub>, diatomite and red-mud [7–17] have been widely investigated as gas explosion inhibitors. The results show that these materials have different inhibition performances on gas explosion. However, to achieve the requirement of practical applications in the coal mines, it is necessary to develop new chemical powders that possess the advantages of low-cost, high efficiency and environmental harmlessness.

Palygorskite clay is a kind of magnesian–aluminum silicate mineral with chain-layer structure [18–20]. China is the largest palygorskite clay origin country in the world. The typical Molecular formula of palygorskite is  $\text{Mg}_5\text{Si}_8\text{O}_{20}(\text{OH})_2(\text{H}_2\text{O})\cdot 4\text{H}_2\text{O}$  [21], which contains different metal ions related to different origins place, such as  $\text{Al}^{3+}$ ,  $\text{Fe}^{3+}$ ,  $\text{Fe}^{2+}$ , etc. In recent years, palygorskite clay has been widely used in industrial fields such as petrochemical industry, environmental protection, food industry, ceramics, insulation materials and plastics [22,23]. In view of its structure, composition and high surface area, palygorskite clay may be feasible for application in the field of gas explosion suppression. However, to the best of our knowledge, there is still no research about the application of palygorskite clay in gas explosion suppression.

Herein, pristine palygorskite powders were used as methane explosion suppression material for the first time. Pristine palygorskite powders were characterized by the techniques of XRD, EDS,  $\text{N}_2$  adsorption-desorption and TG-DSC. The suppression properties of the pristine palygorskite powders for 9.5% methane-air premixed gas were tested in a 20 L spherical explosion vessel and a 5 L pipeline experimental system. Based on the sample characterization results and explosion parameters, the suppression mechanism of the pristine palygorskite powders on the gas explosion was further explored.

## 2. Materials and Methods

### 2.1. Materials

Pristine palygorskite powders, which are gray in color, were obtained from Xuyi, Jiangsu province, China. The samples were dried in a vacuum oven at 50 °C for 2 h, and further ground by an agate mortar. Finally, the pristine palygorskite powders for test were collected through a 200 mesh sieve screen.

### 2.2. Characterization

X-ray diffraction (XRD) analysis was carried on Bruker-AXS D8 (Bruker, Madison, WI, USA) with  $\text{CuK}\alpha$  radiation at 40 kV and 25 mA. Energy dispersive spectra (EDS) were observed by field-emission scanning electron microscopy (FEI, Eindhoven, Netherlands). Thermogravimetry-Differential scanning calorimetry (TG-DSC) analysis was completed on a Simultaneous Thermal Analyzer (NETZSCH, Selb, Germany) in a flow of air ( $20 \text{ mL}\cdot\text{min}^{-1}$ ) at a heating rate of  $10 \text{ }^\circ\text{C}\cdot\text{min}^{-1}$ . In this process the starting temperature was 30 °C and the terminating temperature was 800 °C.  $\text{N}_2$  adsorption-desorption isotherms were obtained on a Quantachrome Autosorb-iQ sorption analyzer (Quantachrome, Boynton Beach, FL, USA). Before the measurement, the samples were degassed at 150 °C for more than 6 h. The specific surface areas ( $S_{\text{BET}}$ ) of the samples were calculated following the multi-point BET (Brunauer-Emmett-Teller) procedure. The pore size distributions were determined from the adsorption branch of the isotherms using the DFT method.

### 2.3. Explosion Experiment Device and test Process

The effects on the methane-air premixed gas explosion pressure of pristine palygorskite powders with different concentration were tested with a 20 L spherical explosion instrument. The system mainly includes explosion vessel, gas flow controller, powder injection system, ignition controller and data acquisition system. The illustration of the 20 L spherical explosion instrument is presented in Figure 1.

The test process was as follows. Firstly, a certain amount of pristine palygorskite powders was placed into the powder storage tank, and then the compressed air was filled until 2 MPa. The 9.5% methane-air gas was premixed by the partial pressure method. The methane was introduced into the explosion vessel to 0.06 MPa. Then, the solenoid valve, which controlled the powder injection, was triggered within 10 ms when the ignition button was pressed, and the injection time was 50 ms. Thus, the ignition time was set at 60 ms delay to ensure that the ignition is simultaneous with the powder injection, and the ignition energy was 105 J. The data were collected and analyzed by the

computer. In the experiment, the explosion pressure tests were repeated 3–5 times under the same conditions until the test results tended to be stable because the powder dispersion inside the 20 L spherical vessel is not uniform [24].

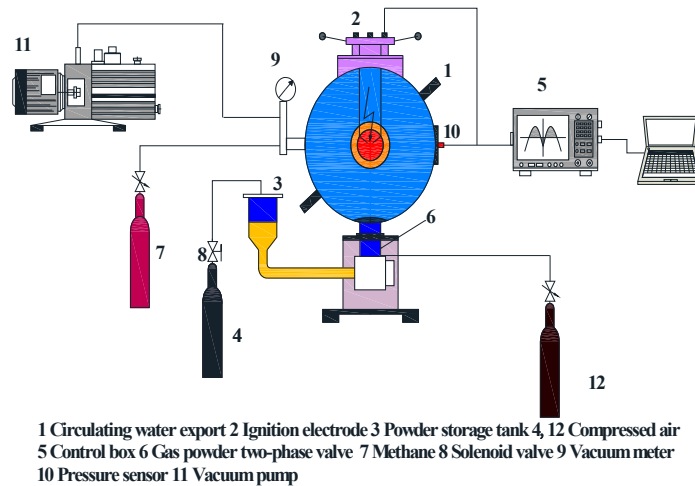


**Figure 1.** The illustration of 20 L spherical explosion system.

The flame propagation velocity was measured by a pipeline explosion system. The illustration of the pipeline explosion system is shown in Figure 2. The system was composed of five parts: explosion pipeline, ignition system, powder injection system, image collection system and gas allocation system. The pipeline was made by Perspex with a cross-sectional area of  $100 \times 100 \text{ mm}^2$  and a length of 500 mm. The testing procedure was as follows. Firstly, a certain amount of pristine palygorskite powders was put into the storage tank, the top of the pipeline was sealed with PVC film, and the volume fraction of methane being introduced into the pipeline was 9.5% by adjusting the flow meter. In the process of gas distribution, the exhaust port was opened, and the mixed gas flow was filled into the pipeline for 5 min to ensure that all the air in the pipeline was discharged. Then, the solenoid valve was triggered by the synchronous controller and the powders were injected into the duct by the 0.3 MPa 9.5% premixed methane-air. After 450 ms ignition delay, the methane-air mixtures in the duct were ignited automatically by the electrical pulse igniter. The entire explosion process was recorded with a high-speed camera at a speed of  $2000 \text{ frames} \cdot \text{s}^{-1}$ . The average velocity of flame propagation was calculated with the distance measured by Photoshop software.

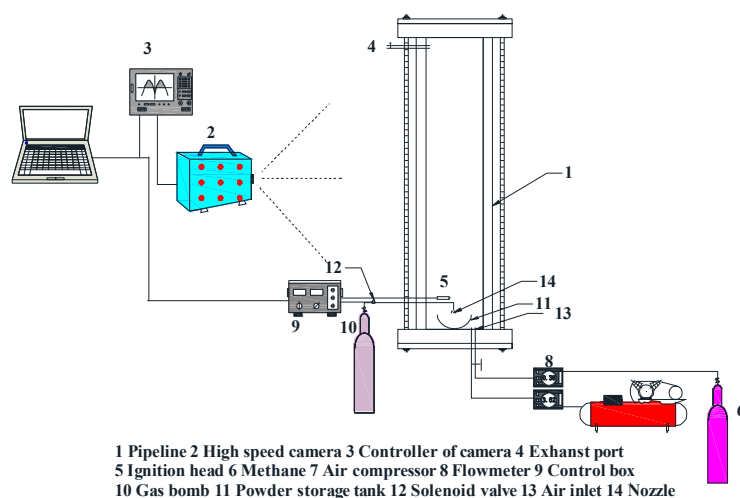


**Figure 2.** The illustration of the pipeline explosion system.

### 3. Results and Discussion

#### 3.1. Characterization of Palygorskite Powders

Figure 3 shows the EDX and element mapping of the pristine palygorskite powders. The composition of the sample is shown in Figure 3a. In this figure, the surface composition (wt.%) of O, Si, C, Al, Fe, Mg, Ca, K and Ti elements on pristine palygorskite powders are 41.6%, 31.6%, 9.1%, 6.3%, 4.2%, 2.9%, 2.7%, 1.2% and 0.4%, respectively. Furthermore, a surface scanning analysis of some elements in EDS is illustrated in Figure 3b. In Figure 3b, the O, Si, C, Al, Fe and Mg elements are simultaneously detected and these elements are highly dispersed on the pristine palygorskite powders surface. The existence of surface oxygen may be due to the adsorption of oxygen in air, however we can still confirm that the main components of the pristine palygorskite powders are in the form of oxides, silicates and carbonates, which is consistent with the result obtained by XRD.

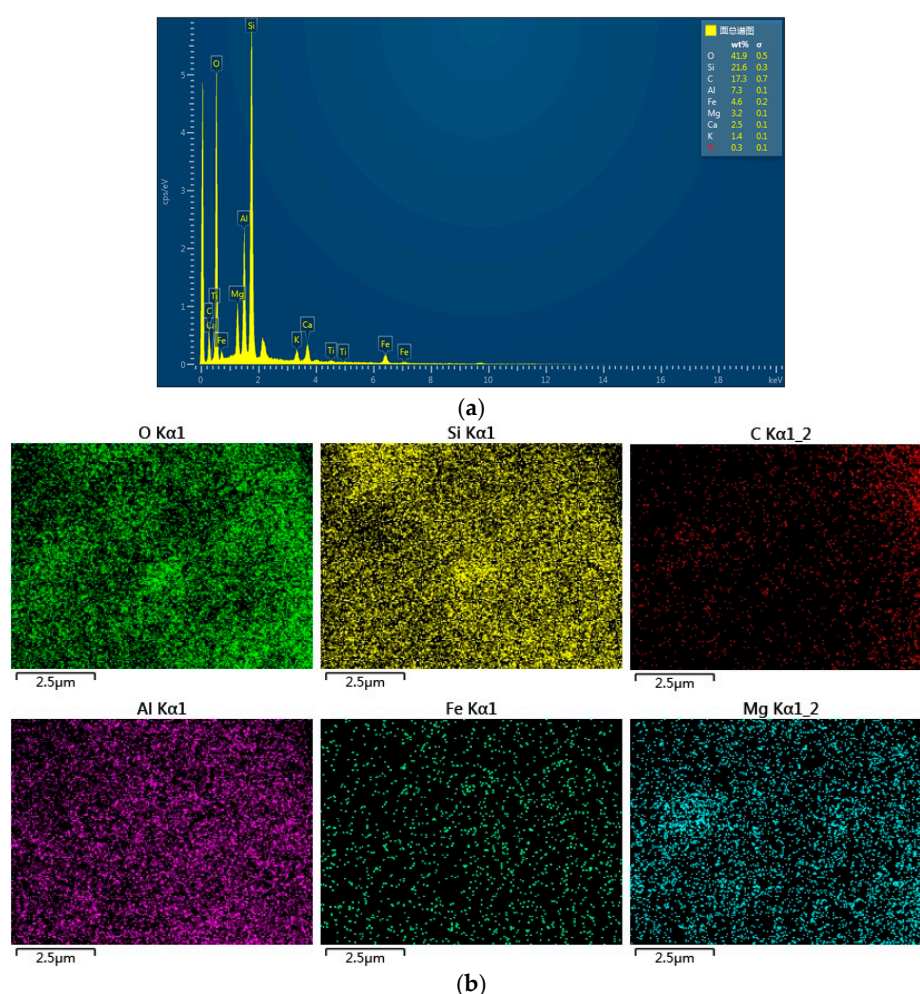


**Figure 3.** Energy dispersive spectra (EDS) of the pristine palygorskite powders (a); and EDS element mappings of the O, Si, C, Al, Fe and Mg elements (b).

The phase analysis of pristine palygorskite powders was carried by X-ray diffractometer, as shown in Figure 4. From the XRD pattern, the diffraction peaks of  $8.49^\circ$  and  $19.89^\circ$  are the characteristic peaks of palygorskite  $((\text{MgAl})_5(\text{SiAl})_8\text{O}_{20}(\text{OH})_2 \cdot (\text{H}_2\text{O})_8)$ . The diffraction peaks appearing at  $20.85^\circ$ ,  $26.63^\circ$ ,  $36.54^\circ$ ,  $50.13^\circ$ ,  $54.87^\circ$  and  $59.95^\circ$  could be attributed to quartz (JCPDS Card:33-1161). The diffraction peaks of  $30.93^\circ$  and  $41.12^\circ$  are characteristic peaks of dolomite  $(\text{MgCa}(\text{CO}_3)_2)$ . The peak at  $29.4^\circ$  is the characteristic diffraction peaks of Calcite  $(\text{CaCO}_3)$ . According to the XRD pattern, the mineralogical

composition of the pristine palygorskite powders was analyzed. The results show that the mass contents of pure palygorskite, quartz, dolomite, garronite, and calcite were approximately 49.2%, 33%, 14.7%, 1.2% and 1.8%, respectively. Therefore, the main components of this sample were pure palygorskite, quartz, and a little amount of dolomite, garronite and calcite.

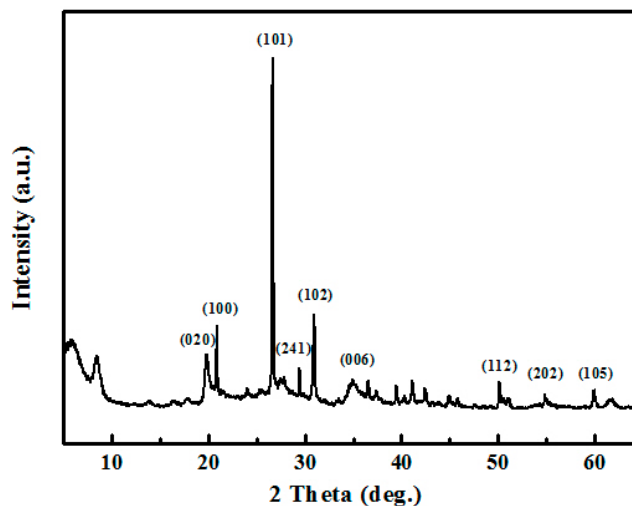


Figure 4. XRD pattern of the pristine palygorskite powders.

Figure 5 displays the  $N_2$  adsorption-desorption isotherm (Figure 5a) and the corresponding pore size distribution curve (Figure 5b) of the pristine palygorskite powders. As shown in Figure 5a, the pristine palygorskite powders showed a typical type IV isotherm with obvious hysteresis loops. Within the range of  $p/p_0 < 0.4$ , the adsorption increased very slowly with the increase of relative pressure, and the adsorption line and desorption line coincide. When  $p/p_0 > 0.4$ , the presence of mesopores and larger pores in the sample caused the capillary condensation in the adsorption process, more and more holes were filled, and the desorption and adsorption branches did not overlap in the high-pressure region. It is precisely because of the capillary condensation that the results of H3 hysteresis loops appeared. The specific surface area of pristine palygorskite powders is  $41.26 \text{ m}^2 \cdot \text{g}^{-1}$ , which was calculated by the method of multi-point BET. From the pore size distribution curve of the pristine palygorskite powders, it can be seen that the pores were distributed in the range of 2–20 nm, indicating the mesoporous structure of the pristine palygorskite powders.

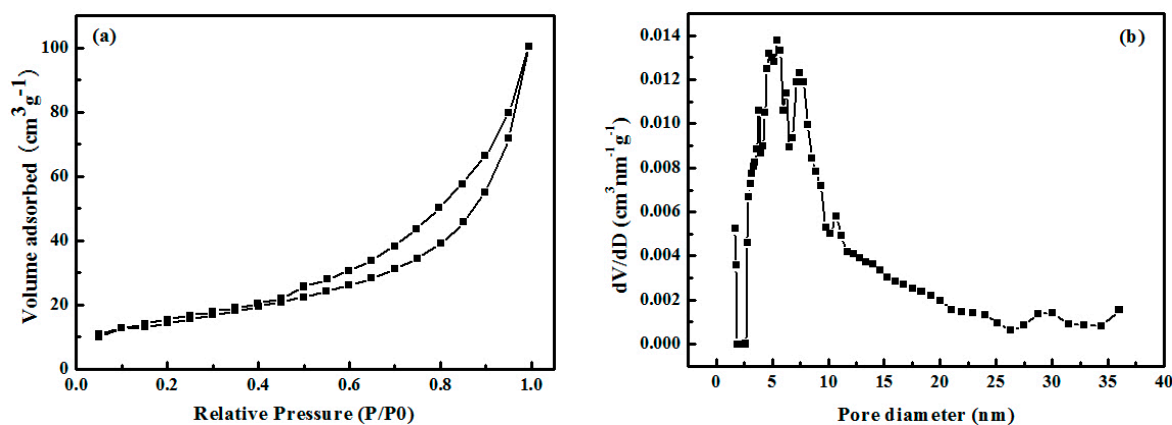


Figure 5.  $N_2$  adsorption-desorption isotherm (a); and the corresponding pore size distribution curve (b) of the pristine palygorskite powders.

The TG-DSC curves of the pristine palygorskite powders are presented in Figure 6. From the TG curve, it can be seen that the pristine palygorskite powders began to lose weight from 30 °C, and the curve stepped with three stages: The first weight loss from 30 to 200 °C was mainly attributed to the decomposition of adsorption water on the surface. The second weight loss from 200 to 500 °C should be attributed to the removal of crystalline water. The third weight loss from 500 to 700 °C was caused by the removal of hydroxy. After 700 °C, the weight of pristine palygorskite powders did not change any more. The total weight loss of the pristine palygorskite powders was 17% throughout the heating process. Corresponding to the TG curve, the DSC curve showed three endothermic peaks. According to integrating the area of the endothermic peaks on the DSC curve, the total endothermic quantity of the pristine palygorskite powders was 250 J·g<sup>-1</sup>, which indicated the sample had an excellent heat absorption performance.

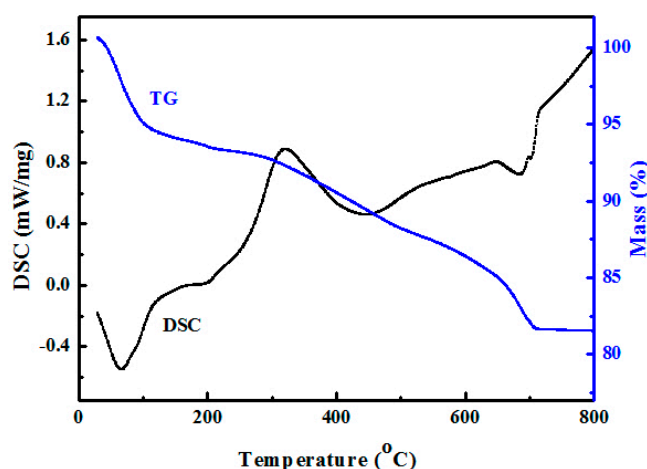
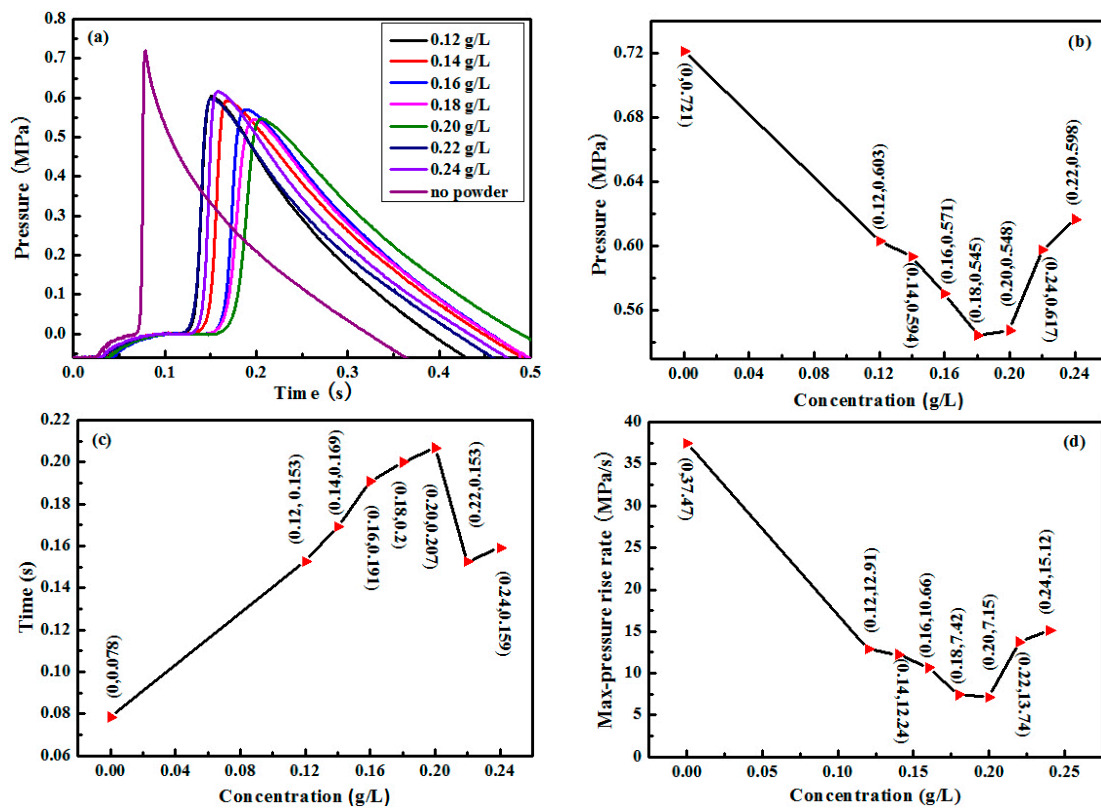


Figure 6. TG-DSC curves of the pristine palygorskite powders.

### 3.2. Suppression Properties of Palygorskite Powders

The suppressions effect of different pristine palygorskite powders concentrations (0.12 g·L<sup>-1</sup>, 0.14 g·L<sup>-1</sup>, 0.16 g·L<sup>-1</sup>, 0.18 g·L<sup>-1</sup>, 0.20 g·L<sup>-1</sup>, 0.22 g·L<sup>-1</sup> and 0.24 g·L<sup>-1</sup>) on the 9.5% methane-air premixed gas explosion are shown in Figure 7. Figure 7a reveals the explosion pressure–time curves after adding pristine palygorskite powders with different concentrations and no powders. In Figure 7a, the max-pressure of methane explosion was reduced to different degrees after adding different concentrations of pristine palygorskite powders, and the times reach explosion max-pressure were delayed obviously. Figure 7b presents the pressure peak values of methane explosion with different concentrations of pristine palygorskite powders. It is seen that the max-pressure of the 9.5% premixed methane-air explosion decreased firstly and then increased with the increase of pristine palygorskite powders concentration. Among them, the max-pressure reached the minimum value of 0.545 MPa. Figure 7c shows the effect of different concentrations of pristine palygorskite powders on the time reaching the explosion max-pressure. The results exhibited that the time reaching the explosion max-pressure was delayed with the concentration increase. When the mass concentration of pristine palygorskite powders was 0.2 g·L<sup>-1</sup>, the time reaching the max-pressure was the longest, 0.207 s. Figure 7d shows the max-pressure rising rate of methane explosion with different concentrations of pristine palygorskite powders, the curves of which were similar to those shown in Figure 7b. The max-pressure rising rate was inhibited to 7.15 MPa·s<sup>-1</sup> when the mass concentration of pristine palygorskite powders was 0.2 g·L<sup>-1</sup>. The above analysis results of several explosive pressure parameters indicate that pristine palygorskite powders with the mass concentration of 0.2 g·L<sup>-1</sup> exhibit the best inhibitory effect on the 9.5% premixed methane-air explosion. When the powder concentration is more than the optimum, the decrease of the inter powder spaces will restrict the

diffusion of temperature to individual powder and powder decomposition, resulting in the decline of the inhibitory effect on the 9.5% premixed methane-air explosion [25].



**Figure 7.** The suppressing effect of pristine palygorskite powders with different concentrations on methane explosion: (a) the curves of explosion pressure; (b) the values of pressure peak; (c) the time on the pressure peak; and (d) the rising rate max-pressure.

To compare the suppression effect of pristine palygorskite powders with other widely used powders, the suppression effect of silica powders with the same mass concentration and particle size distribution were tested in the experiments, and we referred the results of BC and ABC powders with optimal concentration ( $0.1 \text{ g}\cdot\text{L}^{-1}$ ) from the literature [26]. The experimental results of the four powders on the explosion of 9.5% premixed methane-air are shown in Figure 8. The methane explosion can be suppressed to a certain degree with all four kinds of powders. Among them, the inhibitory effect of silica powders was the worst, and that of pristine palygorskite powders was comparable with BC and ABC powders, with almost no difference on the max-pressure of methane explosion. However, for the time reaching the max-pressure, ABC powders were obviously better than BC powders, and BC powders were slightly better than pristine palygorskite powders. Table 1 lists the effects of four different powders on the explosion pressure parameters in detail. In Table 1, compared to no powder, the methane explosion max-pressure for pristine palygorskite powders ( $0.20 \text{ g}\cdot\text{L}^{-1}$ ) decreased from 0.721 MPa to 0.548 MPa, i.e., 25.1%. The time reaching the max-pressure was also delayed from 0.078 s to 0.2 s, which is almost three times longer. When adding the same mass concentration of silica powders, the explosion pressure of methane decreased by only 10.2%, and the time reaching max-pressure was only two times longer than that of no powder. When  $0.1 \text{ g}\cdot\text{L}^{-1}$  BC and ABC powders were added, respectively, the times reaching max-pressure were delayed to 0.28 s and 0.45 s, and the max-pressure decreased by 28.3% and 25.1%. The results indicate that, although the explosion suppression property of pristine palygorskite powders is little lower than that of ABC powders, pristine palygorskite powders are still a potential material for the gas explosion suppression.

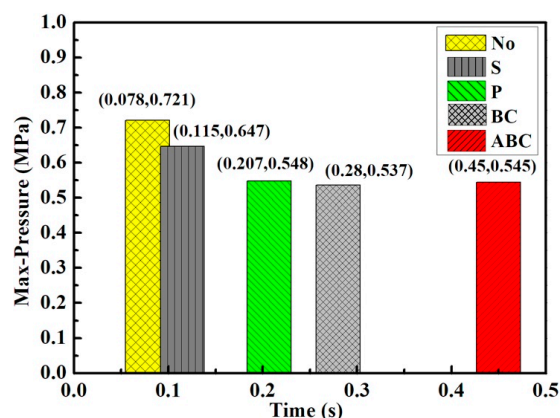


Figure 8. The comparison of the max-pressure and the time reach the max-pressure with different powders.

Table 1. The explosion parameters of methane-air premixed gas with different powders.

Sample	Concentration ( $\text{g}\cdot\text{L}^{-1}$ )	Max-Pressure (MPa)	The Time of Pressure Peak (s)	The rate of Max-Pressure Rise ( $\text{MPa}\cdot\text{s}^{-1}$ )	The ratio of Max-Pressure Drop (%)
No powders	0	0.721	0.078	37.471	0
Palygorskite	0.12	0.603	0.153	12.912	16.3
Palygorskite	0.14	0.594	0.169	12.243	17.6
Palygorskite	0.16	0.571	0.191	10.664	20.8
Palygorskite	0.18	0.545	0.200	7.425	25.1
Palygorskite	0.20	0.548	0.207	7.152	23.9
Palygorskite	0.22	0.598	0.153	13.743	17.1
Palygorskite	0.24	0.617	0.159	15.121	14.4
Silica	0.20	0.647	0.115	23.408	10.2
BC	0.10	0.537	0.28	5.08	28.3
ABC	0.10	0.545	0.45	2.99	25.1

The average velocity of flame propagation was calculated with the image results collected by the pipeline experimental system. Figure 9 displays the suppression effect of the pristine palygorskite powders with different concentrations ( $0.16 \text{ g}\cdot\text{L}^{-1}$ ,  $0.20 \text{ g}\cdot\text{L}^{-1}$ ,  $0.24 \text{ g}\cdot\text{L}^{-1}$  and  $0.28 \text{ g}\cdot\text{L}^{-1}$ ) on the flame propagation velocity of 9.5% premixed methane-air explosion. As shown in Figure 9, after adding pristine palygorskite powders with different concentrations, the average velocity of flame propagation decreased obviously. Moreover, the average velocity of flame propagation decreased with the increase of pristine palygorskite powders concentration when below  $0.24 \text{ g}\cdot\text{L}^{-1}$ . At  $0.24 \text{ g}\cdot\text{L}^{-1}$ , the average velocity of flame propagation was reduced to the minimum. When the powder concentration was more than  $0.24 \text{ g}\cdot\text{L}^{-1}$ , the average velocity of flame propagation increased again.

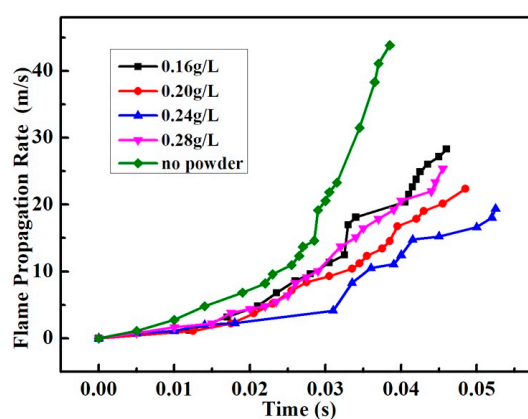
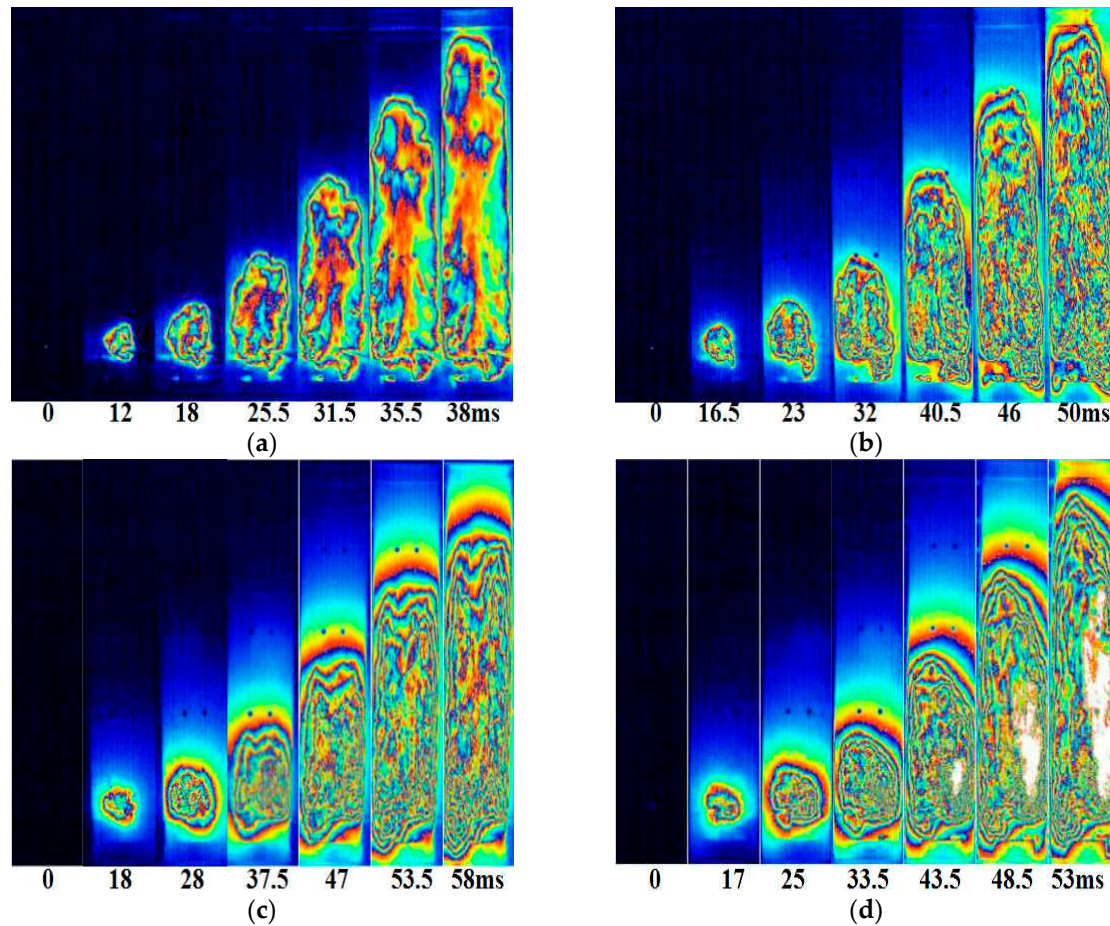


Figure 9. The average velocity of flame propagation of the 9.5% methane-air premixed gas explosion with different concentrations of pristine palygorskite powders.

The flame propagating images of the 9.5% premixed methane-air explosion with pristine palygorskite powders at different concentrations or without powders in the pipeline experimental system are shown in Figure 10. Figure 10a shows the flame propagating images of the methane explosions without pristine palygorskite powders. The time of flame reaching the top of pipeline was 38 ms. Figure 10b–d shows the flame propagating images under pristine palygorskite powders with mass concentrations of  $0.16 \text{ g}\cdot\text{L}^{-1}$ ,  $0.24 \text{ g}\cdot\text{L}^{-1}$  and  $0.28 \text{ g}\cdot\text{L}^{-1}$ , respectively. The flames of methane explosion were delayed obviously after adding the pristine palygorskite powders with different concentrations. When the concentration of pristine palygorskite powders was  $0.24 \text{ g}\cdot\text{L}^{-1}$ , the time of explosion flame propagation reaching the top of pipeline was the longest (58 ms).



**Figure 10.** The flame propagating images of the 9.5% methane-air premixed gas explosion: (a) no powder; (b) with  $0.16 \text{ g}\cdot\text{L}^{-1}$  pristine palygorskite powders; (c) with  $0.24 \text{ g}\cdot\text{L}^{-1}$  pristine palygorskite powders; and (d) with  $0.28 \text{ g}\cdot\text{L}^{-1}$  pristine palygorskite powders.

### 3.3. Suppression Mechanism of Palygorskite Powders

*Physical inhibition effect:* On the one hand, according to the  $\text{N}_2$  adsorption-desorption isotherm, the pristine palygorskite powders were a mesoporous material. The porous powders could fully contact with the free radicals produced by the explosion chain reaction, which increased the wall effect on the destruction of free radicals and caused the explosion chain reaction interrupting [27,28]. On the other hand, the TG-DSC results of pristine palygorskite powders presented three stages of dehydration and decomposition process. Water vapor and carbon dioxide were produced by the thermal process, which not only diluted the oxygen concentration but also absorbed lots of heat generated by the explosion, leading to a good endothermic effect. Therefore, the above two physical effects contributed to the good explosion suppression performance of the pristine palygorskite powders.

**Chemical inhibition effect:** By the energy dispersive spectrum of the pristine palygorskite powders, it was found that the pristine palygorskite powders contained a variety of metal elements. The thermal decomposition products of pristine palygorskite powders, such as MgO, Al<sub>2</sub>O<sub>3</sub> and Fe<sub>3</sub>O<sub>4</sub>, have good thermal stability and good endothermic properties [29,30] and can further react with the free radicals (H·, OH·, and O·) generated by the methane explosion, thus interrupting the explosion chain reaction [31–33].

#### 4. Conclusions

Pristine palygorskite powders were used as the methane explosion suppression material for the first time. Firstly, the pristine palygorskite powders were characterized comprehensively, and the phase analysis results show that the main components of pristine palygorskite powders are pure palygorskite and quartz. The result of N<sub>2</sub> adsorption-desorption indicate that they possess mesoporous structure, and the pores mainly in the range of 2–20 nm. The TG-DSC analysis shows that the pristine palygorskite powders have excellent heat absorption characteristic.

The explosion suppression test results indicate that both the explosion max-pressure and the average velocity of flame propagation of 9.5% methane-air premixed gas decreased firstly and then increased with the increase of the pristine palygorskite powder concentration. The optimum concentration for the pressure suppression was 0.20 g·L<sup>-1</sup>. The max-pressure was reduced by 23.9% and the time reaching the max-pressure was delayed by nearly three times compared to that of no powder. The optimum concentration for the flame propagation suppression was 0.24 g·L<sup>-1</sup>. The explosion suppression properties of pristine palygorskite powders were caused by the synergy of physical and chemical inhibition effects. Based on these experimental results, pristine palygorskite powders could be a desirable and economical inhibitor for the gas explosion suppression. In future research, we will complete the simulation analysis about the computational fluid dynamics and molecular dynamics to further explore the explosion suppression mechanism of palygorskite powders.

**Author Contributions:** Y.Z. conceived and designed the experiments; L.Z., T.Y. and J.G. performed the experiments and analyzed the data; and Y.W. and Z.L. managed all the experimental and writing process as the corresponding authors. All authors discussed the results and commented on the manuscript.

**Funding:** This work was supported by the National Natural Science Foundation of China (51874120, 51504083, 51674104, 51774110, and 51604116), Program for Science & Technology Innovation Talents in Universities of Henan Province (19HASTIT042), Project funded by China Postdoctoral Science Foundation (2016M592290), Natural Science Foundation of Hebei Province of China (E2016508036), the Research Foundation for Youth Scholars of Higher Education of Henan Province (2017GGJS053), the Fundamental Research Funds for the Universities of Henan Province (NSFRF1606), Program for Innovative Research Team in University of Ministry of Education of China (IRT\_16R22), Program for Innovative Research Team of Henan Polytechnic University (T2018-2), Foundation for Distinguished Young Scientists of Henan Polytechnic University (J2017-3) and the State Key Laboratory Cultivation Base for Gas Geology and Gas Control (Henan Polytechnic University) (WS2017A03).

**Conflicts of Interest:** The authors declare no conflict of interest.

#### References

1. Chen, Z.H.; Fan, B.C.; Jiang, X.H. Suppression effects of powder suppressants on the explosions of oxyhydrogen gas. *J. Loss Prev. Process Ind.* **2006**, *19*, 648–655. [[CrossRef](#)]
2. Krasnyansky, M. Prevention and suppression of explosions in gas-air and dust-air mixtures using powder aerosol-inhibitor. *J. Loss Prev. Process Ind.* **2006**, *19*, 729–735. [[CrossRef](#)]
3. Korobeinichev, O.P.; Shmakov, A.G.; Shvartsberg, V.M.; Chernov, A.A.; Yakimov, S.A.; Koutsenogii, K.P.; Makarov, V.I. Fire suppression by low-volatile chemically active fire suppressants using aerosol technology. *Fire Saf. J.* **2012**, *51*, 102–109. [[CrossRef](#)]
4. Pan, R.K.; Xiao, Z.J.; Yu, M.G. The characteristics of methane combustion suppression by water mist and its engineering applications. *Energies* **2017**, *10*, 1566. [[CrossRef](#)]
5. Wang, Z.R.; Ni, L.; Liu, X.; Jiang, J.C.; Wang, R. Effects of N<sub>2</sub>/CO<sub>2</sub> on explosion characteristics of methane and air mixture. *J. Loss Prev. Process Ind.* **2014**, *31*, 10–15. [[CrossRef](#)]

6. Almerinda, D.B.; Francesco, C.; Valeria, D.S.; Ernesto, S. Effect of Diluents on Rapid Phase Transition of Water Induced by Combustion. *AIChE J.* **2012**, *58*, 2810–2819.
7. Liu, Q.M.; Hu, Y.L.; Bai, C.H.; Chen, M. Methane/coal dust/air explosions and their suppression by solid particle suppressing agents in a large-scale experimental tube. *J. Loss Prev. Process Ind.* **2013**, *26*, 310–316. [[CrossRef](#)]
8. Luo, Z.M.; Wang, T.; Ren, J.Y.; Deng, J.; Shu, C.M.; Huang, A.Q.; Cheng, F.M.; Wen, Z.Y. Effects of ammonia on the explosion and flame propagation characteristics of methane-air mixtures. *J. Loss Prev. Process Ind.* **2017**, *47*, 120–128. [[CrossRef](#)]
9. Chen, X.F.; Zhang, H.M.; Chen, X.; Liu, X.Y.; Niu, Y.; Zhang, Y.; Yuan, B.H. Effect of dust explosion suppression by sodium bicarbonate with different granulometric distribution. *J. Loss Prev. Process Ind.* **2017**, *49*, 905–911. [[CrossRef](#)]
10. Zhang, Y.M.; Wang, Y.; Meng, X.Q.; Zheng, L.G.; Gao, J.L. The suppression characteristics of  $\text{NH}_4\text{H}_2\text{PO}_4$ /red mud composite powders on methane explosion. *Appl. Sci.* **2018**, *8*, 1433. [[CrossRef](#)]
11. Wang, Q.H.; Wen, H.; Wang, Q.S.; Sun, J.H. Inhibiting effect of  $\text{Al}(\text{OH})_3$  and  $\text{Mg}(\text{OH})_2$  dust on the explosions of methane-air mixtures in closed vessel. *Sci. China-Technol. Sci.* **2012**, *55*, 1371–1375. [[CrossRef](#)]
12. Zheng, L.G.; Li, G.; Wang, Y.L.; Zhu, X.C.; Pan, R.K.; Wang, Y. Effect of blockage ratios on the characteristics of methane/air explosion suppressed by BC powder. *J. Hazard. Mater.* **2018**, *355*, 25–33. [[CrossRef](#)] [[PubMed](#)]
13. Wang, Y.; Cheng, Y.S.; Yu, M.G.; Li, Y.; Cao, J.L.; Zheng, L.G.; Yi, H.W. Methane explosion suppression characteristics based on the  $\text{NaHCO}_3$ /red-mud composite powders with core-shell structure. *J. Hazard. Mater.* **2017**, *335*, 84–91. [[CrossRef](#)] [[PubMed](#)]
14. Wang, Y.; Cheng, Y.S.; Cao, J.L.; Zheng, L.G.; Yi, H.W.; Yu, M.G. Suppression characteristics of  $\text{KHCO}_3$ /red-mud composite powders with core-shell structure on methane explosion. *J. China Coal. Soc.* **2017**, *42*, 653–658.
15. Koshiba, Y.; Takahashi, Y.; Ohtani, H. Flame suppression ability of metallocenes (nickelocene, cobaltcene, ferrocene, manganocene, and chromicene). *Fire Saf. J.* **2012**, *51*, 10–17. [[CrossRef](#)]
16. Luo, Z.M.; Cheng, F.M.; Wang, T.; Deng, J.; Shu, C.M. Suppressive effects of silicon dioxide and diatomite powder aerosols on coal mine gas explosions in highlands. *Aerosol. Air. Qual. Res.* **2016**, *16*, 2119–2128. [[CrossRef](#)]
17. Cheng, W.M.; Hu, X.M.; Xie, J.; Zhao, Y.Y. An intelligent gel designed to control the spontaneous combustion of coal: Fire prevention and extinguishing properties. *Fuel* **2017**, *210*, 826–835. [[CrossRef](#)]
18. Liang, S.; Lin, Y.J.; Du, Q.G.; Wei, Z.; Yang, Y.L. Preparation and rheology of polyamide-6/attapulgitite nanocomposites and studies on their percolated structure. *Polymer* **2005**, *46*, 5758–5766.
19. He, L.; Zhou, Y.K.; Yan, J.W.; Yang, L. *Modification and Engineering Application of Palygorskite and Its Micro-Nano Materials*; National Defense Industry Press: Beijing, China, 2012.
20. Cao, J.L.; Shao, G.S.; Wang, Y.; Liu, Y.P.; Yuan, Z.Y. CuO catalysts supported on attapulgitite clay for low-temperature CO oxidation. *Catal. Commun.* **2008**, *9*, 2555–2559. [[CrossRef](#)]
21. Pan, M.; Lin, X.M.; Xie, J.J.; Huang, X.M. Kinetic, equilibrium and thermodynamic studies for phosphate adsorption on aluminum hydroxide modified palygorskite nano-composites. *RSC Adv.* **2017**, *7*, 4492–4500. [[CrossRef](#)]
22. Wang, A.Q.; Wang, W.B.; Zheng, Y.A.; Zheng, M.S.; Liu, X.Q. *The Dissociation of Attapulgitite and Its Nano-Functional Composites*; Science Press: Beijing, China, 2014; pp. 62–95.
23. Zheng, M.S.; Wang, A.Q.; Zhan, G.S. *Study on Application of Attapulgitite Caly*; Chemical Industry Press: Beijing, China, 2007; pp. 2–3.
24. Di Sarli, V.; Russo, P.; Sanchirico, R.; Di Benedetto, A. CFD Simulations of the Effect of Dust Diameter on the Dispersion in the 20 L Bomb. *Chem. Eng. Trans.* **2013**, *31*, 727–732.
25. Ranganathan, S.; Rockwell, S.R.; Petrow, D.; Zalosh, R.; Rangwala, A.S. Radiative fraction of dust entrained turbulent premixed flames. *J. Loss Prev. Process Ind.* **2018**, *51*, 65–71. [[CrossRef](#)]
26. Wen, H.; Cao, W.; Wang, K.K.; Cheng, F.M. Experimental study on ABC dry powder to repress gas explosion. *J. Saf. Sci. Technol.* **2010**, *7*, 9–12.
27. Krasnyansky, M. Studies of fundamental physical-chemical mechanisms and processes of flame extinguishing by powder aerosols. *Fire Mater.* **2008**, *32*, 27–47. [[CrossRef](#)]

28. Ni, X.M.; Zheng, Z.; Wang, X.S.; Zhang, S.G.; Zhao, M. Fabrication of hierarchical zeolite 4A microspheres with improved adsorption capacity to bromofluoropropene and their fire suppression performance. *J. Alloys Compd.* **2014**, *592*, 135–139. [[CrossRef](#)]
29. Wang, C.H.; Auad, M.L.; Marcovich, N.E.; Nutt, S. Synthesis and characterization of organically modified attapulgite/polyurethane nanocomposites. *J. Appl. Polym. Sci.* **2008**, *109*, 2562–2570. [[CrossRef](#)]
30. Yao, C.; Zhang, L.L.; Ren, Q.; Li, J.C.; Ding, Y.H. Study on HDPE flame retarded with attapulgite compound intumescent flame retardant. *Plast. Technol.* **2012**, *40*, 37–41.
31. Ni, X.M.; Kuang, K.Q.; Yang, D.L.; Liao, G.X. Experimental study on the suppression of methane/air diffusion flame by iron-modified zeolite powders. *China Saf. Sci. J.* **2012**, *22*, 53–57.
32. Liu, J.H.; Cong, B.H. Experimental evaluation of water mist with metal chloride additives for suppressing CH<sub>4</sub>/Air cup-burner flames. *J. Thermal Sci.* **2013**, *22*, 269–274. [[CrossRef](#)]
33. Ni, X.M.; Wang, X.S.; Zhang, S.G.; Zhao, M. Experimental study on the performance of transition metal ions modified zeolite particles in suppressing methane/air coflowing flame on cup burner. *J. Fire Sci.* **2014**, *32*, 417–430. [[CrossRef](#)]



© 2018 by the authors. Licensee MDPI, Basel, Switzerland. This article is an open access article distributed under the terms and conditions of the Creative Commons Attribution (CC BY) license (<http://creativecommons.org/licenses/by/4.0/>).